

Myofibre Segmentation in Adult Skeletal Muscle using Coherence-Enhancing Diffusion Filtering

Journal:	<i>IEEE Journal of Biomedical and Health Informatics</i>
Manuscript ID:	TITB-00521-2013
Manuscript Type:	Paper
Date Submitted by the Author:	24-Sep-2013
Complete List of Authors:	Strange, Harry; Aberystwyth University, Department of Computer Science Scott, Ian; Nottingham University Hospitals NHS Trust, Department of Cellular Pathology Zwiggelaar, Reyer; Aberystwyth University, Department of Computer Science
TIPS:	Digital Pathology, Image Segmentation, Muscle Biopsy, Coherence-Enhancing Diffusion Filtering

SCHOLARONE™
Manuscripts

Pre-Only

Myofibre Segmentation in Adult Skeletal Muscle using Coherence-Enhancing Diffusion Filtering

Harry Strange, Ian Scott, and Reyer Zwiggelaar

Abstract

The correct segmentation of myofibres in histological muscle biopsy images is a critical step in the automatic analysis process. Errors occurring as a result of incorrect segmentations have a compounding effect on latter morphometric analysis and as such it is vital that the fibres are correctly segmented. This paper presents a new approach to myofibre segmentation based on Coherence-Enhancing Diffusion filtering. This approach is robust to noise and also to weak fibre boundaries. The proposed method is compared against existing state of the art methods and experiments show the effectiveness of the proposed approach. The results show that using the Coherence-Enhancing Diffusion filtering a segmentation accuracy of 90% can be achieved which is an improvement over existing myofibre segmentation techniques.

Index Terms

Digital Pathology, Muscle Biopsy, Image Segmentation, Coherence-Enhancing Diffusion Filtering

I. INTRODUCTION

The examination of stained biopsies from skeletal muscle is a vital component in the diagnostic pathway for the vast majority of neuromuscular disorders and remains essential as a preliminary investigation despite the availability of electron microscopic, genetic and molecular tests for specific conditions.

H. Strange and R. Zwiggelaar are in the Department of Computer Science, Aberystwyth University, Aberystwyth, SY23 3DB, UK. (e-mail: {hgs08,rrz}@aber.ac.uk)

I. Scott is in the Department of Cellular Pathology, Nottingham University Hospitals NHS Trust, Queens Medical Centre, Nottingham, NG7 2UH, UK

Detection of variation in fibre size is seen as a first step in the diagnosis of the majority of neuromuscular disorders including myopathic, dystrophic, neurogenic and inflammatory conditions; examples of which include mitochondrial cytopathies, muscular dystrophies, motor neuron disease, and dermatomyositis [1], [2]. Muscle biopsies in which there is no fibre size variation are most often normal [3]. Further analysis of fibre size variation for those which exhibit a continuous distribution or biopsies showing a biphasic pattern can further assist in obtaining a diagnosis. This data is often difficult to obtain by eye and so there is a need for accurate, automatic methods of analysis of fibre size variation across the full area of the biopsy.

One of the key steps for such automatic methods is the accurate segmentation of the myofibres from the surrounding connective structures (Fig. 1). Inaccuracies in the segmentation of the myofibre boundary will lead to errors at later stages of analysis. As such, there is a real need for automatic segmentation methods that provide accurate results and are robust to different imaging conditions. There are numerous existing approaches to automatic myofibre segmentation ranging from simple thresholding [4] to more advanced methods that use deformable models [5]. The goal of such methods is to accurately segment the myofibre regions from the connective and background regions. This is done by either identifying the pixels in the image associated with the fibres themselves or identifying the boundaries of the fibres — the perimysium and endomysium (see Fig. 1). However, existing methods may fail in cases where there are weak fibre boundaries or an increased presence of noise due to inconsistencies in the staining process.

In this work, Coherence-Enhancing Diffusion (CED) filtering [6] is used to address these problems by enhancing the myofibre boundaries so that the fibres themselves can be accurately segmented. The basic principle of CED filtering is to improve the quality of the flow like structures in an image through the use of anisotropic diffusion tensors. Unlike existing line enhancement methods such as that of Frangi et al. [7], CED filtering uses the structure tensor, along with its principal eigenvectors, to define the orientations for smoothing. CED is therefore well suited to myofibre segmentation as it is robust to noise and can enhance weak fibre boundaries.

II. EXISTING APPROACHES

When performing analysis on myofibre images it is useful to identify the myofibre boundary so that morphometric measures can be obtained. Manual identification and measurement of myofibres can be time consuming, error prone, and can often suffer from intra and inter operator variability. These drawbacks have led to the development of various techniques for automatic myofibre segmentation. The simplest approach is to perform thresholding to segment the image into foreground and background regions, one

1
2
3
4 corresponding to myofibres and the other representing background and connective tissue. The central step
5 of such an approach is the selection of a threshold value to separate the two regions such that they are
6 well represented. Although methods exist to estimate the threshold automatically [8], or manually [4],
7 thresholding is an inefficient method for myofibre segmentation as the fibres cannot be split from the
8 background, or from each other, using a single threshold value. As such, more advanced methods are
9 needed to segment the myofibre regions.

14 These more advanced approaches can be broadly split into two categories: those that use edge detection
15 to identify the perimysium or endomysium (the myofibre boundaries), and those that use deformable
16 models to identify the myofibres. This dichotomy is by no means exclusive as many approaches will use
17 methods from both of these categories.

20 Edge detection methods seek to segment the perimysium and endomysium so that the fibres can be
21 segmented from these boundaries. Therefore, edge detection methods are often used as a pre-processing
22 step to fibre segmentation with the justification being that, if the boundaries are correctly identified, the
23 fibres themselves can be segmented as the interior of the boundary regions. Tzekis et al. [9] presented
24 an ensemble approach to edge detection, with Sobel, Laplacian, and the Mode Colour algorithms being
25 employed in a single framework to attempt to robustly identify the myofibre boundaries. Once identified,
26 the edges could be used as *a priori* information for further segmentation; it is worth noting however that
27 the approach to such a segmentation is not mentioned in the original paper. Sertel et al. [10] present a more
28 established framework that uses edge detection as the first step in myofibre segmentation. Ridge analysis
29 [7] is applied to ATPase stained cross-sections to segment the connective tissue so that thresholding
30 the ridge likelihood image produces a rough segmentation of the connective tissue regions. This rough
31 segmentation is further refined through morphological operations to connect any unconnected components.
32 Small regions are removed and the watershed transform is used to separate any touching boundaries. The
33 results show that using this approach myofibres can be effectively segmented with the added benefit of
34 the algorithm being fast to execute.

46 The second category of segmentation method seeks to apply deformable models, such as active contour
47 models [11], to identify the myofibre regions. Active contour models require a seed point or curve to
48 initialise the segmentation, as such, many of the active contour based methods can be distinguished by
49 the heuristic used to identify the initial seed locations. The simplest approach is to use manual seed
50 locations to identify the central points of the myofibres. Such an approach was presented by Klemenčič
51 et al. [12], where the user manually identifies the central regions of each myofibre. A Voronoi polygon
52 is then formed from these centroids and a modified active contour model is applied to refine the Voronoi
53
54
55
56
57
58
59
60

1
2
3 polygons so that they ‘fit’ the myofibres. An attempt to automate that initialisation process was made by
4 Röhrle et al. [5] who used the Hough transform to identify circular regions in the image. This method
5 is however sensitive to noise and a parameterisation of the acceptable range of circular radii is needed.
6
7 The limitations of standard active contour models was addressed by Kim et al. [13] where a level set
8 approach was applied to improve the active contour segmentations. Level sets were used to extend the
9 active contour framework by incorporating colour and texture information. As well as this, the initial
10 contour is estimated using a heuristic thresholding approach to overcome the problem associated with
11 manually identifying seed positions. A recent approach by Mula et al. [14] uses Gradient Vector Flow
12 (GVF) to delineate myofibre boundaries. GVF seeks to improve upon active contour modelling by using
13 the gradient vector flow of an image to pull the active contour towards the object boundary. The GVF
14 based myofibre segmentation method initially uses ridge detection to enhance the boundaries before seed
15 locations are automatically chosen by identifying concave areas. The GVF deformable model is then
16 applied to segment the myofibre regions.
17
18
19
20
21
22
23
24
25

26 One the main limitations of the above methods is that they can often fail in cases where noise is
27 introduced as a result of the staining or sectioning process, and also in cases with weak boundaries.
28 As well as this, there is no previous work that directly compares the different approaches to myofibre
29 segmentation in adult cases. Motivated by these drawbacks, this paper presents a method for myofibre
30 segmentation based on Coherence-Enhancing Diffusion filtering that is robust to noise and weak fibre
31 boundaries, and also provides a side by side comparison with the main approaches to the segmentation
32 problem.
33
34
35
36
37
38

39 III. METHODOLOGY

40
41 This work uses Coherence-Enhancing Diffusion (CED) filtering to segment the boundary regions whose
42 interiors contain the myofibres. CED filtering [6] seeks to smooth a degraded original image along
43 the directions determined by the image’s structures through the use of diffusion tensors [15]. Existing
44 nonlinear diffusion filters use a scalar diffusivity rather than a diffusion tensor [16], [17], and as such,
45 they can be regarded as isotropic filters. CED allows for true anisotropic diffusion by building on the
46 work of Cottet and Germain [18] and examining the eigenvalues and eigenvectors of the diffusion tensor.
47 This means that the smoothing process locally adapts and allows smoothing in different directions. This
48 makes CED well suited for myofibre segmentation as it allows for the intrafibre regions (i.e. those regions
49 contained “within” a myofibre) to remain coherent whilst enhancing the connective structures such as
50 the perimysium and endomysium.
51
52
53
54
55
56
57
58
59
60

Figure 2 shows an example image, with the CED image, the resultant myofibre boundaries, and the final segmentation.

A. Pre-processing

The first step is to apply a stain decomposition method [19] to the muscle sections so that processing is performed on only the eosinophilic structures — in this case myofibres — thus excluding any nuclear regions from the segmentation process. This stain decomposition step ensures that the most prominent structures in the image are the myofibres themselves rather than any satellite nuclei. Once the stain decomposition step is performed the image is converted to grayscale and the contrast is enhanced using an adaptive histogram equalisation method [20].

B. Coherence-Enhancing Diffusion (CED) Filters

The central step of CED is to determine the directions along which the image should be smoothed, this is achieved by utilising the eigendecomposition of the second moment matrix, or structure tensor. As explained in [15], the heart of anisotropic diffusion filtering using a diffusion tensor is the evolution of an image using

$$\frac{\delta u}{\delta t} = \nabla \cdot (D \nabla u) \quad (1)$$

where $u(x, t)$ is the image under evolution at diffusion time t . The diffusion tensor, D , is a positive semidefinite matrix which is adapted to the local image structure. The local image structure can be measured using the structure tensor [15], [21] which is defined as

$$J_\rho(\nabla u_\sigma) = G_\rho * (\nabla u_\sigma \nabla u_\sigma^T) \quad (2)$$

where u_σ is defined as u convolved with a Gaussian with standard deviation σ such that $u_\sigma = G_\sigma * u$. As such, u_σ is a regularised version of u obtained via convolution with a Gaussian G_σ . The standard deviation, σ , can be thought to represent the *noise scale* since it forces the edge detector to ignore details smaller than $O(\sigma)$ [6]. The standard deviation, ρ , defines the *integration scale* which describes the characteristic size of the texture [15]. The eigenvectors of J_ρ describe the local orientations, or coherence orientations, and the eigenvalues describe the average contrast along the eigendirections. The eigenvalues of $J_\rho = \begin{pmatrix} J_{11} & J_{12} \\ J_{12} & J_{22} \end{pmatrix}$ are

$$\mu_1 = \frac{1}{2} \left(J_{11} + J_{22} + \sqrt{(J_{11} - J_{22})^2 + 4J_{12}^2} \right)$$

$$\mu_2 = \frac{1}{2} \left(J_{11} + J_{22} - \sqrt{(J_{11} - J_{22})^2 + 4J_{12}^2} \right)$$

These eigenvalues are used to assemble the eigenvectors of the diffusion tensor D . The diffusion tensor of coherence-enhancing diffusion uses the same eigenvectors as J_ρ and the eigenvalues are assembled such that

$$\lambda_1 := c_1 \tag{3}$$

$$\lambda_2 := \begin{cases} c_1, & \text{if } \mu_1 = \mu_2 \\ c_1 + (1 - c_1 \exp(\frac{-c_2}{(\mu_1 - \mu_2)^2})), & \text{otherwise} \end{cases} \tag{4}$$

where $c_1 \in (0, 1)$ serves as a regularisation parameter that ensures that the diffusion tensor remains uniformly positive definite, and $c_2 > 0$ serves as a threshold parameter.

The solution to Eq. 1 can be obtained numerically by utilising finite differences using a time step of size, τ , as the difference between two calculated time levels. For full details on the implementation of coherence-enhancing diffusion filtering the reader is pointed towards Section 5 of [6] and Section 2.2 and 3 of [15].

C. Post-processing

Once the Coherence-Enhancing Diffusion filtering method described above has completed, the final stage of the segmentation process is to use the boundaries identified using CED to segment the myofibre regions. The resultant image produced from CED can be thought as a probability map describing the likelihood of a pixel belonging to a boundary region. As such, to convert the given image into a binary segmentation a thresholding method is used to identify only the pixels corresponding to boundary regions [8]. Following a similar methodology to [10], once the boundary segmentation has been produced, connected components with a total area of less than 750 pixels are removed and morphological closing [22] is used to join together any disconnected boundary regions. For the closing operation a disk structuring element of radius 4 pixels is used. The complement of this binary image then gives the segmentation of the myofibres. The final step is to apply a watershed transformation [23] to split any touching fibres.

IV. DATA

The muscle tissue, obtained following open or Bergstrom needle biopsy, was frozen onto cork blocks and sectioned with the fibres orientated in the transverse plane ($5 - 7\mu m$) using a frozen cryostat (Leica CW1900, Leica GmbH, Germany). The sections were then placed on glass slides and stained with haematoxylin and eosin (H & E) using standard protocols [3]. Entire sections, obtained from 10 anonymised normal adult patients, were scanned at $400\times$ magnification using a NanoZoomer Digital Pathology System (Hamamatsu Photonics UK) and the resulting images viewed using NDP Software (NDP.view 2, Hamamatsu Photonics UK). The final image data used for experimentation was taken as regions of interest measuring 1300×1030 pixels viewed at $10\times$ zoom and stored as uncompressed TIFF files. A total of 2832 fibres were identified across the region of interest images.

The ground truth data was generated by a single user tracing the boundaries of the fibres across all images. In order to validate the manual segmentations as ground truth, a repeatability study was performed whereby the same image was segmented 10 times by the same person. This process resulted in multiple ground truth regions which were then co-registered using a group-wise registration algorithm [24] to obtain an aligned 'mean image'. The absolute difference between each manual segmentation and the mean image was then computed to obtain an overall measure of the ground truth repeatability error. The error was measured as the number of pixels in the difference image divided by the total number of pixels in the original manual segmentation mask. The average error across all 10 cases was measured as $0.056(\pm 0.010)$. This error is low enough to accept the manual segmentations as a good representative of ground truth as it shows that the estimated error in the manual segmentations is only 0.056.

V. METHODOLOGY

To test the effectiveness of the proposed method it is tested against various existing myofibre segmentation algorithms using different measures of accuracy. Multiple evaluation criteria need to be employed as a single measure of accuracy is not appropriate and could lead to an unfair or biased view of an algorithm's performance. As such, multiple criteria are used to build a bigger picture of the effectiveness of a segmentation algorithm. As well as this, the effect of each of the proposed method's parameters are investigated and discussed.

A. Evaluation Criteria

For each method, the segmentation accuracy is measured using both image segmentation evaluation criteria and clinical morphometric measures.

1) *Segmentation Accuracy*: The overall segmentation accuracy of a given method is measured as the number of correctly segmented myofibres (in relation to the given ground truth) divided by the total number of true positive, false positive and false negative regions. To ensure that a segmented myofibre is not counted across multiple regions, a one-to-one mapping is enforced between the ground truth and the automatic segmentations. Each ground truth region is mapped to a single segmented region that is encompassed within the ground truth boundary. Any remaining regions are then counted as false positives.

2) *Fragmentation and Congealment*: To evaluate whether or not the different algorithms over or under segment the myofibre regions two new measures are proposed: *fragmentation* and *congealment*. Fragmentation is used to measure to what extent an algorithm fragments a myofibre in the output segmentation. Given the ground truth segmentations and the output segmentation, fragmentation is defined as $F = p/n$, where p is the total number of fragmented fibres in the output segmentation and n is the total number of fibres in the ground truth. The fragmented fibres are found by counting the number of connected components within a masked region of the output segmentation with the mask being set as each fibre in the ground truth segmentation. Congealment is measured in a similar fashion to fragmentation, however, the purpose of congealment is to measure the number of segmentations that span across multiple fibre boundaries. As such, congealment is defined as $C = q/n$, where q is the total number of congealed fibres in the output segmentation and n is the total number of fibres in the ground truth. A congealed fibre is found by counting the number of connected components within a masked region in the ground truth segmentation with the masks corresponding to the regions in the output segmentation.

For both fragmentation and congealment a value of 0 indicates a low fragmentation or congealment factor. As the value increases, the quality of the segmentation decreases since the algorithm is seen to fragment or congeal the segmentation.

3) *Morphometric Measures*: The two morphometric measures used to evaluate the segmentation algorithms are mean fibre diameter and the variability coefficient [3]. The mean fibre diameter is measured as the length of the minor axis of the segmented fibre region. The minor axis is used as this is the measurement least affected by any kinking of the muscle as a result of processing or by any obliquity of the plane of section [2]. The variability coefficient is used to measure the amount of variability among the fibres and is defined as

$$VC = \frac{1000\tilde{\sigma}}{\tilde{\mu}} \quad (5)$$

where $\tilde{\sigma}$ and $\tilde{\mu}$ are the standard deviation and mean respectively of the set of all fibre diameters for a

given segmentation method. A variability coefficient of less than 250 is considered to be normal and any value above this is then considered abnormal [3]. Since the dataset is drawn from a normal population the variability coefficient should be less than 250.

B. Parameter Considerations

The initial parameters for the CED algorithm were set according to the values laid out and discussed in [15] and subsequently tuned to improve the results. The initial parameter estimates were, $\tau = 1$, $\sigma = 1 \times 10^{-4}$, $\rho = 4$, $c_1 = 1 \times 10^{-10}$, $c_2 = 0.001$. The relative influence of each parameter was then assessed by varying the value of each parameter and assessing the change in the accuracy of the segmentation. A generalised linear regression model [25] was then fitted to the data to assess the relative influence of each parameter. The results are displayed in Table I. Only the integration scale, ρ , has a medium influence on the final segmentation quality. This is not surprising as ρ controls the characteristic size of the texture regions [15]. As such, selecting a sub-optimal value of ρ will lead to either a lack of coherence within myofibres such that the “noisy” aspects within the fibres are not smoothed, or the coherence-enhancement occurs over too large a scale so the fibre boundary details are destroyed. As can be seen in Table I, all other parameters have a relatively low influence on the final segmentation quality.

VI. RESULTS AND DISCUSISON

The proposed method is compared against basic thresholding [8], ensemble of line detectors [9], line enhancement using Frangi filters [7], level sets [26], and active contours [27]. The segmentations obtained from all methods are post-processed to remove any segmented fibres on the boundary of the image. As well as this, any segmented region smaller than 750 pixels in area is removed and a watershed segmentation is performed to split any touching fibres. This ensures that the segmentations are in keeping with the ground truth and also enables more accurate morphometric measurements to be taken. It also ensures that the comparisons are focused on the core algorithms as opposed to any post-processing method used. It is worth noting that the majority of works published on myofibre segmentation include these post-processing steps (e.g. [10], [13]).

The results of performing myofibre segmentation on the data described in Section IV are displayed in Table II and show the efficacy of the proposed Coherence-Enhanced Diffusion (CED) filtering method for myofibre segmentation. The results in Table II show that the CED method achieves a higher segmentation accuracy with a lower standard deviation. This suggests that the proposed method is more robust to the variation in appearance of fibres within the dataset. Many images within the dataset will contain

fibres with weak boundaries and prominent myofibrils which is equivalent to “noisy” regions. When the myofibre regions are well defined with a strong endomysium or perimysium then all methods are able to segment the myofibres adequately. However, the data contains many examples where the myofibres are heterogeneous in appearance, due to problems with the staining (See Fig. 3). Of the total 2814 fibres, 1222 were identified as ‘low’ noise, 882 were identified as ‘medium’ noise, and 710 were identified as ‘high’ noise. Table III shows the performance of the different algorithms under these three conditions. As can be seen, under low noise conditions all algorithms, except thresholding, perform well with accuracies of over 80% with little variation. However, under medium noise the performance of all algorithms drops and under high noise all algorithms, except the proposed CED method, drop to below 65%. CED is still able to accurately segment 81% of the fibres under high noise conditions. This is in contrast to the next best performer, level sets, which achieves an accuracy of 62% under high noise conditions. The reason for CED’s performance can be attributed to the algorithm’s ability to reduce noise *within* a myofibre whilst seeking to enhance the boundary lines. This means that it is less likely to fragment or congeal the fibres. Although the proposed CED method does not have the lowest fragmentation or congealment value, it does have the lowest combined fragmentation and congealment score of 0.18 (see Table II). The next best performer is active contours with a combined fragmentation and congealment value of 0.26. This shows that the proposed method is able to provide a robust segmentation with regions not being over or under segmented. This is in contrast to the worst performing method, thresholding, where some regions are badly fragmented or heavily congealed. A high value of both fragmentation and congealment indicates that the method is sensitive to heterogeneous areas, and so fragments these areas, and also to weak fibre boundaries leading to large congealed areas.

When considering the clinical metrics, all methods achieve a mean diameter that is within the standard deviation range of the ground truth segmentations (See Table II). Moreover, when examining the histogram of fibre diameters all algorithms produce histograms with the majority of fibres falling in the $50\mu m$ to $80\mu m$ range. This is in keeping with the expectation of the data set as the data is drawn from adult male cases [3]. Two-sample Kolmogorov-Smirnov tests were used to check whether the distributions of fibre diameters from the ground truth and each segmentation algorithm were drawn from the same continuous distribution. In all cases the null hypothesis was rejected meaning that the distribution of fibre diameters for each segmentation algorithm closely matched that of the ground truth.

Since all methods achieve a similar average fibre diameter, what is of more interest is the differences in the variability coefficient. As explained in Section V, the variability coefficient is a measure of the variation in fibre diameters across all segmented regions. As shown in Eq. 5, the variability coefficient

1
2
3
4 assigns more prominence to the standard deviation of the measurements and so a method that has a large
5 amount of variation will obtain a high variability coefficient score. It is noted that a variability coefficient
6 score of below 250 is counted as normal [3], and since the data is drawn from a normal population all
7 algorithms are expected to produce results with a variability coefficient of less than 250. This is validated
8 by the ground truth which has a variability coefficient of $230.31(\pm 40.07)$. The proposed method has a
9 variability coefficient of $251.85(\pm 59.74)$ which, although not below 250, is close enough to be counted
10 as within range as it is less than 5% of the standard deviation out from the mark of 250. All other
11 methods have a variability coefficient of greater than 300 which indicates abnormal cases, even though
12 the data is normal. The reason for this large variability coefficient can be attributed to high fragmentation
13 and congealment factors which lead to outliers within the segmentations as shown in Table II.

14
15 To further analyse the differences in variability coefficient, a Mann-Whitney U test [28] was employed
16 to test the null hypothesis that the distribution of variability coefficients for the ground truth and automatic
17 methods are drawn from continuous distributions with equal medians. The null hypothesis would be
18 rejected at the 0.05 level when there is no significant difference between the two distributions. All
19 automatic methods apart from Coherence-Enhancing Diffusion filtering had the null hypothesis rejected,
20 meaning that the distributions of variability coefficient between the ground truth and CED are statistically
21 similar.

22 23 24 25 26 27 28 29 30 31 32 33 34 35 36 37 38 39 40 41 42 43 44 45 46 47 48 49 50 51 52 53 54 55 56 57 58 59 60

A. Failure Cases

The segmentation in Fig. 4 shows a case where the proposed CED method fails to adequately segment the myofibres. Two fibres in particular are badly segmented due to a weak boundary between the fibres. Although parts of each of the fibre have been identified, they are not useful for subsequent analysis and so count as a failure case. The reasons for such bad segmentation can be attributed to the fact that a single set of parameters are defined for the CED equations across all types of images. As mentioned previously, histological muscle biopsy images can be obstructed by the presence of noise due to incorrect staining or section handling, as such a single set of parameters may not be able to adequately account for all the variation in the data. It would be beneficial for future research to be focussed on providing an adaptive parameter methodology to handle such scenarios.

VII. CONCLUSIONS

A new method for myofibre segmentation in adult skeletal muscle cases has been presented based on Coherence-Enhancing Diffusion (CED) filtering. This proposed method allows for the myofibre boundaries

to be enhanced whilst maintaining the coherence of the pixels within a myofibre region. When compared against existing methods for myofibre segmentation such as level sets, active contours, and line enhancement, CED is able to achieve superior segmentation accuracies of approximately 90%. As well as this, through the use of morphometric features such as mean fibre diameter and the variability coefficient, the proposed CED method is able to closely match ground truth segmentations and produce results that are clinically consistent. Future work will be focused on applying the proposed CED algorithm to abnormal cases so as to build a complete framework for myofibre segmentation and abnormality detection. Moreover, morphometric measurements will be used to automatically identify clinically interesting aspects such as atrophy and hypertrophy factors as well as fibre type proportions and prominence. However, to achieve this the proposed method will need to be tested and evaluated on ATPase stained sections. As well as this, future research will investigate employing CED filtering to whole slide images so as to obtain an estimate of fibre size variation across the full area of the biopsy.

ACKNOWLEDGMENTS

This work was partially funded by the NISCHR Biomedical Research Unit for Advanced Medical Imaging and Visualisation.

REFERENCES

- [1] D. S. Younger, Ed., *Motor Disorders*. Lippincott Williams & Wilkins, 1999.
- [2] M. H. Brooke and W. K. Engel, "The histographic analysis of human muscle biopsies with regard to fibre types: I adult male and female," *Neurology*, vol. 19, pp. 221–223, 1969.
- [3] V. Dubowitz and C. A. Sewry, *Muscle Biopsy: A Practical Approach*. Saunders, 2006.
- [4] P. Karen, M. Števanec, V. Smerdu, E. Cvetko, L. Kubínová, and I. Eržen, "Software for muscle fibre type classification and analysis," *European Journal of Histochemistry*, vol. 53, no. 2, pp. 87–95, 2009.
- [5] O. Röhrle, H. Köstler, and M. Loch, "Segmentation of skeletal muscle fibres for applications in computational skeletal muscle mechanics," Stuttgart Research Centre for Simulation Technology, Tech. Rep., 2011.
- [6] J. Weickert, "Coherence-enhancing diffusion filtering," *International Journal of Computer Vision*, vol. 31, pp. 111–127, 1999.
- [7] A. Frangi, W. J. Iessen, K. L. Vincken, and M. A. Viergever, "Multiscale vessel enhancement filtering," in *Proceedings of the 1st International Conference on Medical Image Computing and Computer-Assisted Intervention (MICCAI)*, 1998.
- [8] N. Otsu, "A threshold selection method from gray-level histograms," *IEEE Transactions on Systems, Man, and Cybernetics*, vol. 9, no. 1, pp. 62–66, 1979.
- [9] P. Tzekis, A. Papastergiou, A. Hatzigaidas, and A. Cheva, "A sophisticated edge detection method for muscle biopsy image analysis," in *Proceedings of the 7th WSEAS International Conference on Signal, Speech and Image Processing*, 2007.
- [10] O. Sertel, B. Dogdas, C. S. Chiu, and M. N. Gurcan, "Microscopic image analysis for quantitative characterization of muscle fiber type composition," *Computerized Medical Imaging and Graphics*, vol. 35, pp. 616–628, 2011.

- 1
2
3
4 [11] M. Kass, A. Witkin, and D. Terzopoulos, "Snakes - active contour models," *International Journal of Computer Vision*,
5 vol. 1, no. 4, pp. 321–331, 1987.
- 6 [12] A. Klemenčič, S. Kovačič, and F. Pernuš, "Automated segmentation of muscle fiber images using active contour models,"
7 *Cytometry*, vol. 32, pp. 317–326, 1998.
- 8 [13] Y.-J. Kim, T. Brox, W. Feiden, and J. Weickert, "Fully automated segmentation and morphometrical analysis of muscle
9 fiber images," *Cytometry Part A*, vol. 71A, pp. 8–15, 2007.
- 10 [14] J. Mula, J. D. Lee, F. Liu, L. Yang, and C. A. Peterson, "Automated image analysis of skeletal muscle fiber cross-sectional
11 area," *Journal of Applied Physiology*, vol. 114, no. 1, pp. 148–155, 2013.
- 12 [15] J. Weickert and H. Schar, "A scheme for coherence-enhancing diffusion filtering with optimized rotation invariance,"
13 *Journal of Visual Communication and Image Representation*, vol. 13, pp. 103–118, 2002.
- 14 [16] P. Perona and J. Malik, "Scale space and edge detection using anisotropic diffusion," *IEEE Transactions on Pattern Analysis
15 and Machine Intelligence*, vol. 12, pp. 629–639, 1990.
- 16 [17] J. Weickert, "A review of nonlinear diffusion filtering," in *Proceedings of the First International Conference on Scale-Space
17 Theory in Computer Vision*. Springer, 1997, pp. 3–28.
- 18 [18] G. Cottet and L. Germain, "Image processing through reaction combined with nonlinear diffusion," *Mathematics of
19 Computation*, vol. 61, pp. 659–673, 1993.
- 20 [19] A. Rabinovich, S. Agarwal, C. A. Laris, J. H. Price, and S. Belongie, "Unsupervised color decomposition of histologically
21 stained tissue samples," in *Proceedings of the Seventh Annual Conference on Neural Information Processing Systems
22 (NIPS)*, 2003.
- 23 [20] K. Zuiderveld, *Graphic Gems IV*. Academic Press, 1994, ch. Contrast Limited Adaptive Histogram Equalization.
- 24 [21] J. Bigün and G. H. Granlund, "Optimal orientation direction of linear symmetry," in *Proceedings of the First International
25 Conference on Computer Vision (ICCV '87)*, 1987.
- 26 [22] P. Soille, *Morphological Image Analysis: Principals and Applications*. Springer-Verlag New York, Inc., 2004.
- 27 [23] L. Najman and M. Schmitt, "Watershed of a continuous function," *Signal Processing (Special issue on Mathematical
28 Morphology)*, vol. 38, pp. 99–112, 1994.
- 29 [24] E. Learned-Miller, "Data drive image models through continuous joint alignment," *IEEE Transactions on Pattern Analysis
30 and Machine Intelligence*, vol. 28, no. 2, pp. 236–250, 2006.
- 31 [25] J. Nedler and R. Wedderburn, "Generalized linear models," *Journal of the Royal Statistical Society*, vol. 125, no. 3, pp.
32 370–384, 1972.
- 33 [26] Y. Zhang, B. J. Matuszewski, L. K. Shard, and C. J. Moore, "Medical image segmentation using new hybrid level-set
34 method," in *Proceedings of the IEEE International Conference on Biomedical Visualisation (MEDi08VIS)*, 2008.
- 35 [27] T. F. Chan and L. A. Vese, "Active contours without edges," *IEEE Transactions on Image Processing*, vol. 10, no. 1, pp.
36 266–277, 2001.
- 37 [28] H. B. Mann and D. R. Whitney, "On a test of whether one of two random variables is stochastically larger than the other,"
38 *Annals of Mathematical Statistics*, vol. 18, no. 1, pp. 50–60, 1947.
- 39
40
41
42
43
44
45
46
47
48
49
50
51
52
53
54
55
56
57
58
59
60



Harry Strange received the B.Eng. degree in software engineering in 2008 and the Ph.D. degree in computer science in 2011 from Aberystwyth University. He is currently a research associate in medical image analysis at the Department of Computer Science, Aberystwyth University. His current research interests include mammographic image analysis, pathology informatics, manifold learning, and texture-based segmentation.

Ian Scott (BSc, MD, DPhil, FRCPath) is a Consultant Neuropathologist for the Nottingham University Hospitals NHS Trust working at the Queen's Medical Centre, Nottingham.



Reyer Zwiggelaar received the Ir. degree in applied physics from the State University Groningen, Groningen, The Netherlands, in 1989, and the Ph.D. degree in electronic and electrical engineering from University College London, London, U.K., in 1993. He is currently a Professor at the Department of Computer Science, Aberystwyth University, U.K. He is the author or co-author of more than 150 conference and journal papers. He is Associate Editor of the Journal of Biomedical and Health Informatics (formerly IEEE Transactions on Information Technology in BioMedicine). His current research interests include medical image understanding, especially focusing on mammographic and prostate data, pattern recognition, statistical methods, texture-based segmentation, and feature-detection techniques.

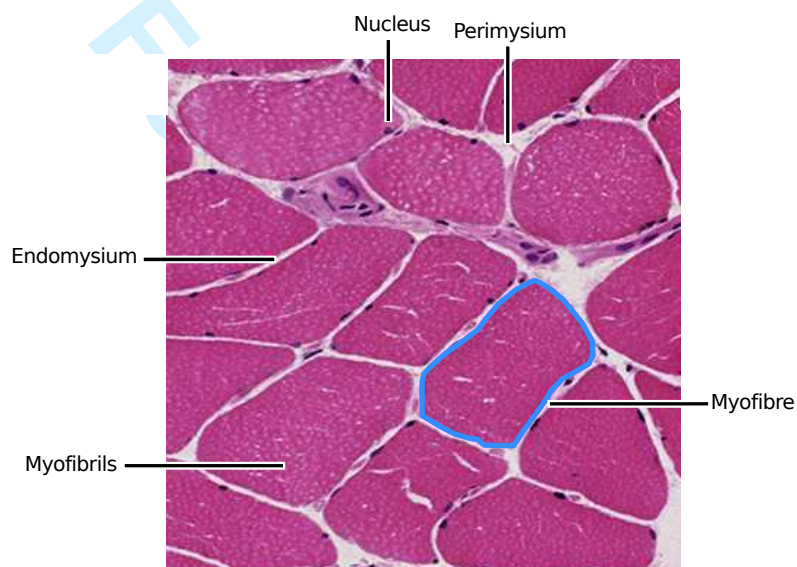


Fig. 1. General organisation of skeletal muscle. Polygonal myocytes are shown revealing the presence of peripheral nuclei. The stained sarcoplasm within the myofibrils is light pink. Each fibre is surrounded by mesenchymal matrix known as the endomysium. Myocytes are grouped into fascicles invested by a connective tissue sheath known as perimysium. The perimysium contains nerves and blood vessels that supply the muscle.

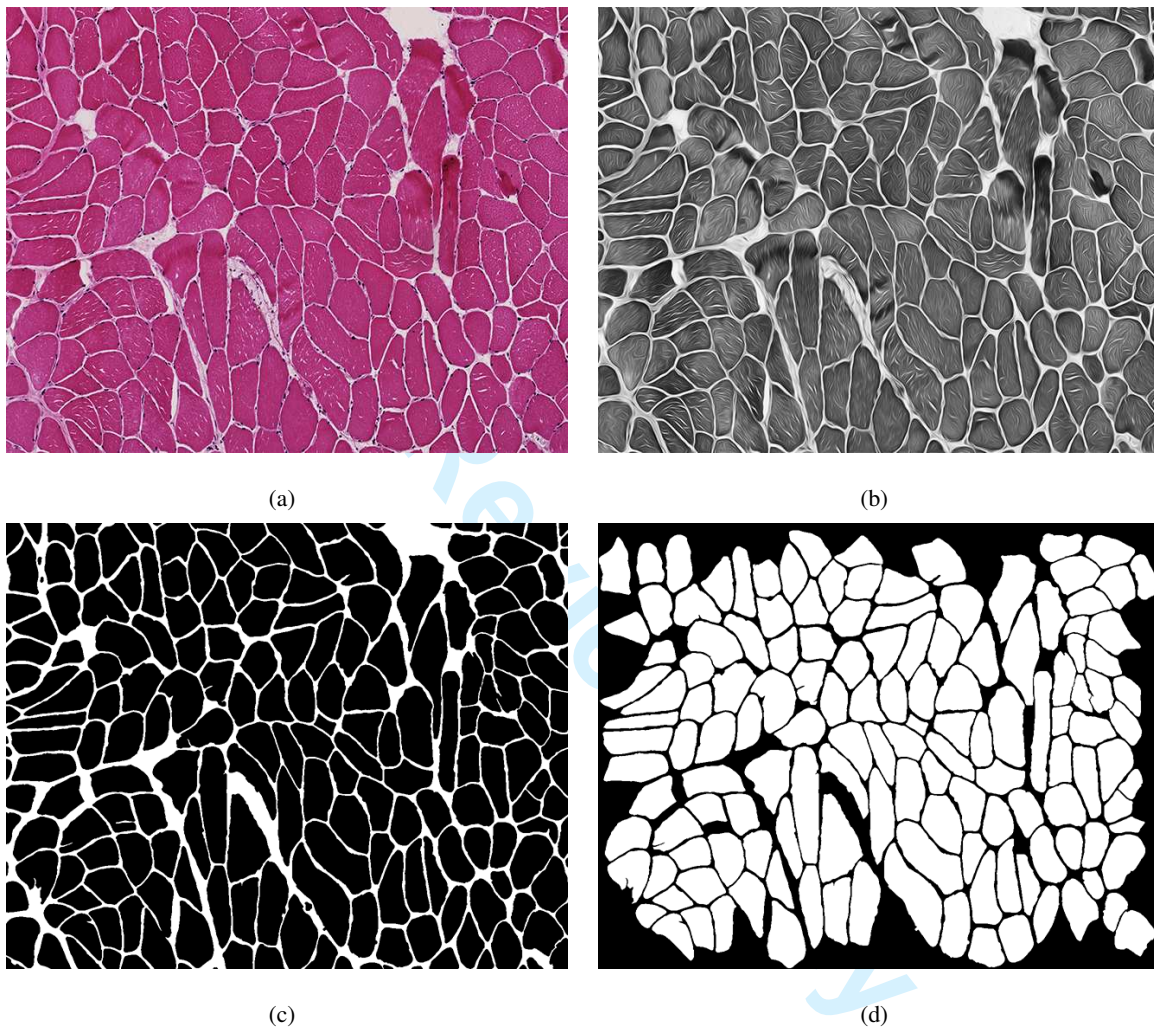


Fig. 2. The section in (a) shows a haematoxylin and eosin (H & E) stained ROI from an adult normal case. (b) shows the image produced as a result of coherence-enhancing diffusion filtering. The myofibre boundaries have been enhanced whilst smoothing the regions within the fibres themselves. The resulting boundary segmentation is shown in (c) and the final segmentation after post-processing is shown in (d).

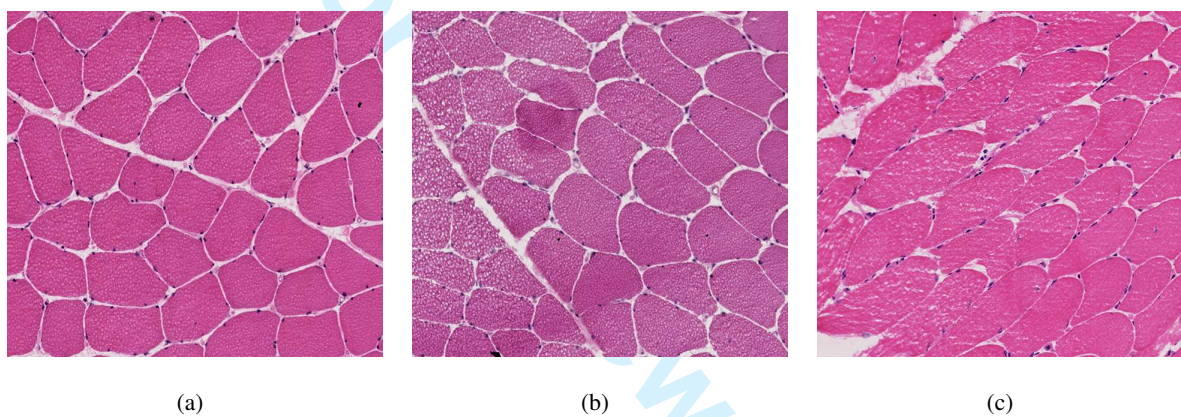


Fig. 3. Example cases drawn from the set of (a) low, (b) medium, and (c) high noise cases. As shown in Table III, most methods will perform well on the low noise cases, but the presence of noise within the myofibrils combined with weak fibre boundaries (b, c) can lead to poor segmentation results.

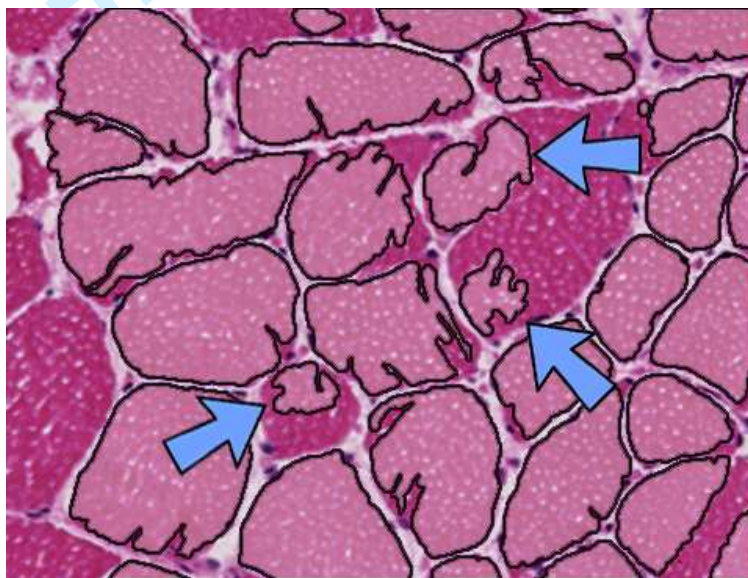


Fig. 4. An example region of interest from a larger section where inadequate segmentations can occur for the proposed CED method. The blue arrows indicate myofibers that are poorly segmented and could lead to inaccurate morphometric measurements.

TABLE I

A DESCRIPTION OF THE DIFFERENT PARAMETERS EMPLOYED FOR COHERENCE-ENHANCED DIFFUSION FILTERING ALONG WITH THEIR RELATIVE INFLUENCE.

Parameter	Description	Influence
τ	Size of diffusion time step	Low
σ	Noise scale (Eq. 2)	Low
ρ	Integration scale (Eq. 2)	Medium
c_1	Regularisation Parameter (Eq. 3)	Low
c_2	Eigenvalue threshold parameter (Eq. 3)	Very Low
t_{area}	Minimum fibre area threshold	Low

TABLE II
QUANTITATIVE RESULTS FOR EACH SEGMENTATION ALGORITHM

	Fibre Acc. (%)	Fragmentation	Congealment	Mean Diameter (μm)	VC (μm)
Thresholding	67.9 (± 21)	0.43 (± 0.30)	0.35 (± 0.28)	60.53 (± 21.75)	337.10 (± 92.60)
Line Detectors	68.2 (± 20)	0.08 (± 0.11)	0.19 (± 0.13)	66.01 (± 22.32)	336.00 (± 139.22)
Vesselness Enhancement	64.0 (± 23)	0.28 (± 0.19)	0.07 (± 0.12)	53.40 (± 19.63)	312.84 (± 58.2)
Level Sets	77.0 (± 18)	0.09 (± 0.09)	0.18 (± 0.13)	63.41 (± 21.48)	327.64 (± 105.00)
Active Contours	73.0 (± 16)	0.06 (± 0.08)	0.20 (± 0.13)	66.41 (± 22.21)	325.03 (± 103.71)
Proposed Method	89.9 (± 9)	0.08 (± 0.07)	0.10 (± 0.11)	62.83 (± 18.31)	251.85 (± 59.74)
Ground Truth				59.21 (± 15.58)	230.31 (± 40.07)

TABLE III

FIBRE SEGMENTATION ACCURACIES OBTAINED AFTER SPLITTING THE DATA INTO THREE GROUPS ACCORDING TO THE 'NOISE' LEVEL OF EACH IMAGE.

	Low (%)	Medium (%)	High (%)
Thresholding	79.7(± 0.11)	77.2(± 0.16)	48.5(± 0.17)
Line Detectors	81.4(± 0.13)	79.2(± 0.15)	48.6(± 0.10)
Vesselness	85.8(± 0.07)	65.4(± 0.20)	46.1(± 0.20)
Level Sets	87.3(± 0.09)	84.7(± 0.08)	62.4(± 0.21)
Active Contours	84.0(± 0.11)	79.8(± 0.12)	57.8(± 0.10)
Proposed Method	95.9(± 0.02)	91.1(± 0.04)	81.1(± 0.09)